





On the self-constraint mechanism of the cross-stream secondary flow in a streamwise-rotating channel

Cite as: Phys. Fluids **32**, 105115 (2020); <https://doi.org/10.1063/5.0023695>

Submitted: 31 July 2020 . Accepted: 28 September 2020 . Published Online: 09 October 2020

 Z. Yang (杨子轩),  B.-Q. Deng (邓冰清),  B.-C. Wang, and  L. Shen



View Online



Export Citation



CrossMark

ARTICLES YOU MAY BE INTERESTED IN

[Direct numerical simulation on the effects of surface slope and skewness on rough-wall turbulence](#)

Physics of Fluids **32**, 105113 (2020); <https://doi.org/10.1063/5.0024038>

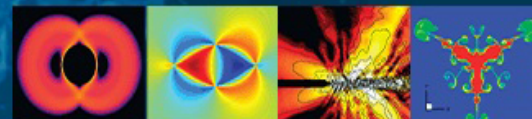
[On the wake flow behind a sphere in a pipe flow at low Reynolds numbers](#)

Physics of Fluids **32**, 103605 (2020); <https://doi.org/10.1063/5.0017349>

[Large scale structures of turbulent flows in the atmospheric surface layer with and without sand](#)

Physics of Fluids **32**, 106604 (2020); <https://doi.org/10.1063/5.0023126>

Physics of Fluids
GALLERY OF COVERS



On the self-constraint mechanism of the cross-stream secondary flow in a streamwise-rotating channel

Cite as: Phys. Fluids 32, 105115 (2020); doi: 10.1063/5.0023695

Submitted: 31 July 2020 • Accepted: 28 September 2020 •

Published Online: 9 October 2020



Z. Yang (杨子轩),^{1,2}  B.-Q. Deng (邓冰清),^{3,a)}  B.-C. Wang,⁴  and L. Shen³ 

AFFILIATIONS

¹State Key Laboratory of Nonlinear Mechanics, Institute of Mechanics, Chinese Academy of Sciences, Beijing 100190, China

²School of Engineering Sciences, University of Chinese Academy of Sciences, Beijing 100190, China

³Department of Mechanical Engineering and St. Anthony Fall Laboratory, University of Minnesota, Minneapolis, Minnesota 55455, USA

⁴Department of Mechanical Engineering, University of Manitoba, Winnipeg, Manitoba R3T 5V6, Canada

^{a)}Author to whom correspondence should be addressed: bdeng@umn.edu

ABSTRACT

The mechanism underlying the magnitude-reverse phenomenon of the mean spanwise velocity with respect to an increasing rotation number in a streamwise-rotating channel flow is investigated through a budget balance analysis of Reynolds shear stress $\langle u'_2 u'_3 \rangle$. It is found that $\langle u'_2 u'_3 \rangle$ imposes a negative feedback to itself through the production term, which prevents its magnitude from increasing monotonically with an increasing rotation number. This behavior of $\langle u'_2 u'_3 \rangle$ further leads to the magnitude reverse in the spanwise wall shear stress and mean spanwise velocity in the near-wall region.

Published under license by AIP Publishing. <https://doi.org/10.1063/5.0023695>

I. INTRODUCTION

Turbulent channel flows subjected to streamwise system rotation feature a distinct mean spanwise motion, of which the direction changes three times between the two walls of the channel, forming a “double S-shaped” profile^{1–9} (see Fig. 1). In laminar flows, the mean spanwise velocity is found to be the primary secondary flow from an instability analysis.¹⁰ In turbulent flows, the spanwise velocity is correlated with the Reynolds shear stress $\langle u'_2 u'_3 \rangle$, which is zero in non-rotating channel flows, but becomes non-trivial in streamwise-rotating channel flows. In this paper, subscripts 1–3 denote the streamwise, wall-normal, and spanwise directions, respectively, the prime denotes the fluctuations, and a pair of angular brackets $\langle \cdot \rangle$ denote averaging over time and homogeneous directions, i.e., the x_1 - and x_3 -directions.

An important feature of the mean spanwise velocity $\langle u_3 \rangle$ in the streamwise-rotating channel flow is the non-monotonic behavior of its magnitude with respect to an increasing rotation number.^{4,11} To be specific, at low rotation numbers, the magnitude of $\langle u_3 \rangle$ increases

with the rotation number. However, there exists a critical rotation number, above which the magnitude of $\langle u_3 \rangle$ decreases as the rotation number continues to increase. Although such a reverse effect of the rotation number on the mean spanwise velocity is shown in many previous studies, the investigation of the underlying mechanism is limited.

The transport equations of Reynolds stresses, which reflect the contributions of different physical processes to the budget balances of turbulent kinetic energy and momentum fluxes, are useful for understanding the flow dynamics.^{12–16} For example, the sustaining mechanism of the large-scale roll cells in the streamwise-rotating channel, namely, the Taylor–Görtler-like vortices, is elucidated through the investigation of the energy transport processes.¹⁷ In this paper, we explore the underlying mechanism of the non-monotonic behavior of the mean spanwise velocity. The remainder of this paper is organized as follows. In Sec. II, the database used for the present study is described. In Sec. III, the non-monotonic behaviors of the magnitudes of $\langle u_3 \rangle$ and $\langle u'_2 u'_3 \rangle$ with respect to the rotation number increase are demonstrated. The mechanism

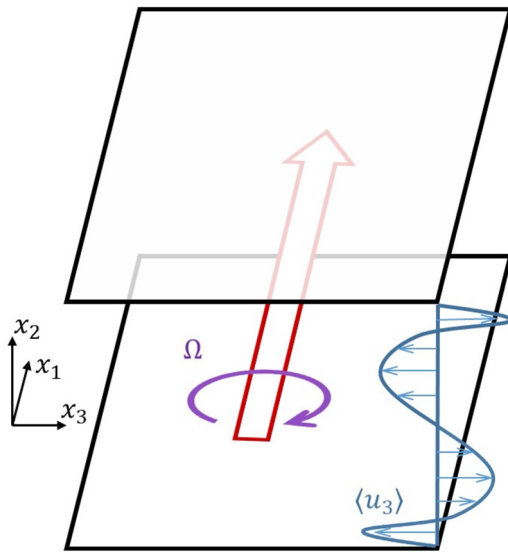


FIG. 1. Schematic of a turbulent channel flow subjected to a streamwise system rotation. The red hollow arrow points to the streamwise direction. The angular velocity of the system rotation is Ω . The streamwise system rotation induces a mean spanwise secondary flow $\langle u_3 \rangle$, which changes its direction three times between the two channel walls.

underlying the magnitude-reverse effect of the rotation number on $\langle u_3 \rangle$ and $\langle u'_2 u'_3 \rangle$ is investigated through the analyses of the balance equation of mean spanwise shear stress and the transport equation of $\langle u'_2 u'_3 \rangle$ in Sec. IV, followed by a summary of major conclusions in Sec. V.

II. DATABASE OF STREAMWISE-ROTATING CHANNEL FLOW

The present study is conducted based on the database of streamwise-rotating channel flows established by Yang and Wang¹⁸ using direct numerical simulation (DNS). The governing equation of the DNS is expressed as

$$\frac{\partial u_i}{\partial x_i} = 0, \quad (1)$$

$$\frac{\partial u_i}{\partial t} + u_k \frac{\partial u_i}{\partial x_k} = -\frac{1}{\rho} \frac{\partial p}{\partial x_i} + \nu \frac{\partial^2 u_i}{\partial x_k \partial x_k} - 2\varepsilon_{ilk} \Omega u_k - \frac{\Pi}{\rho} \delta_{il}, \quad (2)$$

where ρ and ν represent the density and kinematic viscosity of the fluid, respectively, p is the pressure, Ω is the angular velocity of the streamwise system rotation, Π is a constant mean streamwise pressure gradient that drives the flow, and ε_{ijk} and δ_{ij} are Levi-Civita symbol and the Kronecker delta, respectively. A pseudo-spectral method code is utilized to solve Eqs. (1) and (2). A detailed description of the numerical algorithm is given in the work of Yang and Wang.¹⁸

Table I summarizes the key parameters of the DNS data. As shown, the rotation number $Ro_\tau = 2\Omega h/u_\tau$ ranges from 0 to 150, where $u_\tau = \sqrt{\Pi h/\rho}$ is the wall-friction velocity, while the Reynolds

TABLE I. Key parameters, computational domain, and grid resolution of DNS cases.

Ro_τ	Ro_c	Re_τ	Re_c	$L_1 \times L_2 \times L_3$	$N_1 \times N_2 \times N_3$
0	0	180	3263	$16\pi h \times 2h \times 8\pi h$	$512 \times 128 \times 512$
7.5	0.44	180	3068	$32\pi h \times 2h \times 8\pi h$	$1024 \times 128 \times 512$
15	0.97	180	2784	$64\pi h \times 2h \times 8\pi h$	$2048 \times 128 \times 512$
30	2.17	180	2488	$128\pi h \times 2h \times 8\pi h$	$4096 \times 128 \times 512$
75	6.20	180	2177	$256\pi h \times 2h \times 8\pi h$	$8192 \times 128 \times 512$
150	12.92	180	2090	$512\pi h \times 2h \times 8\pi h$	$16384 \times 128 \times 512$

number is fixed at $Re_\tau = u_\tau h/\nu = 180$. The values of the corresponding mean-velocity-based rotation number $Ro_c = 2\Omega h/U_c$ and Reynolds number $Re_c = U_c h/\nu$ are also given in the table, where U_c is the mean velocity at the channel center. The criteria for determining the computational domain size L_i and number of grid points N_i are discussed in detail in the work of Yang and Wang.¹⁸ In summary, as the rotation number increases, a larger streamwise domain size L_1 with a larger number of grid points N_1 is needed to capture the streamwise-elongated vortex structures, of which the characteristic streamwise scale extends as the rotation number increases. The longest computational domain used in the DNS is $L_1 = 512\pi h$ for the case of $Ro_\tau = 150$. In contrast, the characteristic spanwise scale of the large-scale vortices remains almost unchanged at various rotation numbers such that $L_3 = 8\pi h$ with $N_3 = 512$ is fixed in all cases. In our previous studies, the DNS data were analyzed to investigate the effect of streamwise system rotation on the pressure field¹⁹ and the sustaining mechanism of large-scale vortices.¹⁷ In the present study, we focus on investigating the non-monotonic dynamic behavior of the magnitude of the cross-stream secondary flow in response to the increase in the rotation number.

III. EFFECT OF ROTATION NUMBER ON MEAN SPANWISE VELOCITY

Figure 2 compares the profiles of the mean spanwise velocity $\langle u_3 \rangle^+$ at six rotation numbers. In this paper, the superscript “+” denotes variables non-dimensionalized using ν/u_τ and u_τ as characteristic length and velocity scales, respectively. Given that the profiles of $\langle u_3 \rangle^+$ are antisymmetric about the central plane ($x_2/h = 0$) of the channel, they are only displayed in the lower half of the channel (for $-1 \leq x_2/h \leq 0$). From the inset graph, which shows the profile of $\langle u_3 \rangle^+$ at $Ro_\tau = 150$ across the entire channel, it is seen that the sign of $\langle u_3 \rangle^+$ changes three times between two channel walls, resulting in four distinct layers of opposite motions. The magnitude of the near-wall negatively valued peak of $\langle u_3 \rangle^+$ (located at $x_2/h = -0.96$ to -0.89) reaches its maximum at $Ro_\tau = 30$. The magnitude-reverse phenomenon of $\langle u_3 \rangle^+$ occurring at $Ro_\tau \approx 30$ observed in Fig. 2 is consistent with the findings of Weller and Oberlack⁴ and Yang, Su, and Wu,¹¹ who reported that the magnitude of $\langle u_3 \rangle^+$ reverses around $Ro_\tau = 14$ – 30 at similar Reynolds numbers.

To further investigate the non-monotonic behavior of the mean spanwise velocity, we perform time and plane averaging on the third-component of Eq. (2) and integrate the resultant equation in the x_2 -direction, leading to the following balance equation of the

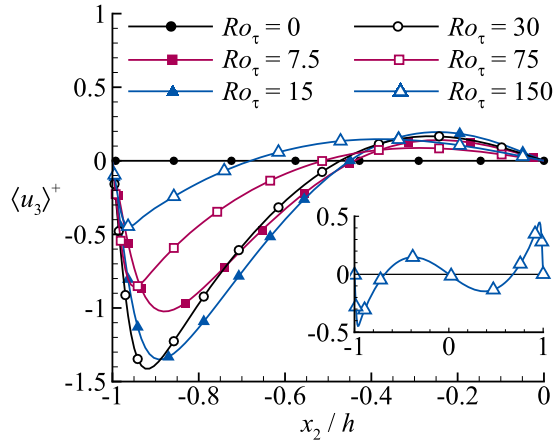


FIG. 2. Profiles of mean spanwise velocity $\langle u_3 \rangle^+$ at various rotation numbers. In order to demonstrate the structures of secondary mean flow, the profile of mean spanwise velocity $\langle u_3 \rangle^+$ at $Ro_\tau = 150$ is also displayed across the entire channel ($-1 \leq x_2/h \leq 1$) in an inset graph, which shows a characteristic pattern of four distinct layers of opposite motions.

spanwise shear stress:

$$\frac{d\langle u_3 \rangle^+}{dx_2^+} = \langle u'_2 u'_3 \rangle^+ + \tau_{23}^{\text{wall}+}, \quad (3)$$

where $\tau_{23}^{\text{wall}+} = (d\langle u_3 \rangle^+/dx_2^+)_{x_2^+ = -h^+}$ represents the spanwise wall shear stress. Equation (3) shows a linear relationship between $d\langle u_3 \rangle^+/dx_2^+$ and $\langle u'_2 u'_3 \rangle^+$, suggesting that it would be helpful to examine the profiles of $\langle u'_2 u'_3 \rangle^+$ to understand the non-monotonic behavior of the magnitude of $\langle u_3 \rangle^+$.

Figure 3 compares the profiles of Reynolds stresses $\langle u'_2 u'_3 \rangle^+$ at six rotation numbers. As expected, the variation in the peak value of $\langle u'_2 u'_3 \rangle^+$ is also non-monotonic with respect to an increasing rotation number. The magnitude of $\langle u'_2 u'_3 \rangle^+$ is the largest at $Ro_\tau = 30$ among all cases under investigation. The reverse effects of the rotation number on the magnitudes of $\langle u_3 \rangle^+$ and $\langle u'_2 u'_3 \rangle^+$ are intriguing.

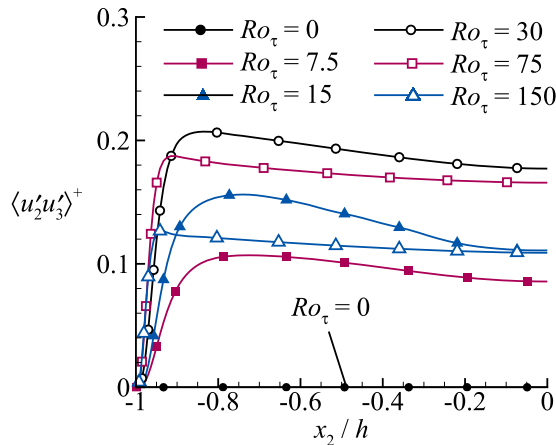


FIG. 3. Profiles of Reynolds stresses $\langle u'_2 u'_3 \rangle^+$ at various rotation numbers.

In Sec. IV, these phenomena are further investigated by seeking their physical explanations through the budget analysis of the Reynolds shear stress $\langle u'_2 u'_3 \rangle^+$.

IV. SELF-CONSTRAINT MECHANISM OF REYNOLDS SHEAR STRESS $\langle u'_2 u'_3 \rangle^+$

In this section, the non-monotonic behaviors of $\langle u_3 \rangle^+$ and $\langle u'_2 u'_3 \rangle^+$ are further investigated through the analysis of the transport equation of the Reynolds stress $\langle u'_i u'_j \rangle$, expressed as

$$\frac{\partial \langle u'_i u'_j \rangle}{\partial t} = 0 = P_{ij} + C_{ij}^{\text{eff}} + \Pi_{ij}^c + \varepsilon_{ij} + T_{ij} + D_{ij}. \quad (4)$$

Here, P_{ij} , C_{ij}^{eff} , Π_{ij}^c , ε_{ij} , T_{ij} , and D_{ij} denote the production term, effective rotation term, convection-induced pressure term, dissipation term, turbulent diffusion term, and viscous diffusion term, respectively, defined as

$$P_{ij} = - \left(\langle u'_i u'_k \rangle \frac{\partial \langle u_j \rangle}{\partial x_k} + \langle u'_j u'_k \rangle \frac{\partial \langle u_i \rangle}{\partial x_k} \right), \quad (5)$$

$$C_{ij}^{\text{eff}} = 2\Omega(\varepsilon_{1ik} \langle u'_j u'_k \rangle + \varepsilon_{1jk} \langle u'_i u'_k \rangle) - \frac{1}{\rho} \left\langle u'_i \frac{\partial p'_r}{\partial x_j} + u'_j \frac{\partial p'_r}{\partial x_i} \right\rangle, \quad (6)$$

$$\Pi_{ij}^c = - \frac{1}{\rho} \left\langle u'_i \frac{\partial p'_c}{\partial x_j} + u'_j \frac{\partial p'_c}{\partial x_i} \right\rangle, \quad (7)$$

$$\varepsilon_{ij} = -2\nu \left\langle \frac{\partial u'_i}{\partial x_k} \frac{\partial u'_j}{\partial x_k} \right\rangle, \quad (8)$$

$$T_{ij} = - \frac{\partial \langle u'_i u'_j u'_k \rangle}{\partial x_k}, \quad (9)$$

$$D_{ij} = \nu \frac{\partial^2 \langle u'_i u'_j \rangle}{\partial x_k \partial x_k}. \quad (10)$$

In Eq. (6), the effective rotation term consists of two parts, namely, the Coriolis term C_{ij} and the rotation-induced pressure term Π_{ij}^r , which are defined, respectively, as

$$C_{ij} = 2\Omega(\varepsilon_{1ik} \langle u'_j u'_k \rangle + \varepsilon_{1jk} \langle u'_i u'_k \rangle), \quad (11)$$

$$\Pi_{ij}^r = - \frac{1}{\rho} \left\langle u'_i \frac{\partial p'_r}{\partial x_j} + u'_j \frac{\partial p'_r}{\partial x_i} \right\rangle. \quad (12)$$

The Coriolis term C_{ij} , as noted in many previous studies of rotating flows,^{18,20–24} represents the effect of the system rotation on the transport equations of Reynolds stresses. The rotation-induced pressure term, which is usually absorbed into the pressure term in previous studies, should be also regarded as a direct consequence caused by the imposed system rotation. This point can be explained by the definition of the rotation-induced pressure given below.

In Eqs. (7) and (12), the pressure p is decomposed into a convection-induced part p^c and a rotation-induced part p^r . The convection-induced pressure p^c is governed by the following Poisson equation and boundary conditions:

$$\begin{cases} \frac{1}{\rho} \frac{\partial^2 p^c}{\partial x_i \partial x_i} = - \frac{\partial u_i}{\partial x_j} \frac{\partial u_j}{\partial x_i}, \\ \text{with } \frac{\partial p^c}{\partial x_2} = \rho \nu \frac{\partial^2 u_2}{\partial x_2^2} \text{ at } x_2 = \pm h, \end{cases} \quad (13)$$

while the Poisson equation and boundary condition for the rotation-induced pressure p_r are expressed as

$$\left\{ \begin{array}{l} \frac{1}{\rho} \frac{\partial^2 p_r}{\partial x_i \partial x_i} = 2\Omega\omega_1, \\ \text{with } \frac{\partial p_r}{\partial x_2} = 0 \quad \text{at } x_2 = \pm h. \end{array} \right. \quad (14)$$

The above decomposition of pressure was proposed in our previous study of the effect of system rotation on the pressure field.¹⁹ This method for pressure decomposition is not only rigorous in mathematics but also conceptually clear in flow physics by separating the non-rotating and rotating effects on the pressure field. The rotation-induced pressure p_r is a direct consequence of the imposed streamwise system rotation, and therefore, the Coriolis term C_{ij} and the rotation-induced pressure term Π_{ij}^r are combined as an effective rotation term C_{ij}^{eff} in Eq. (6) for the analysis of the budget of Reynolds stresses. In our previous study of the sustaining mechanism of Taylor–Görtler-like vortices,¹⁷ similar transport equations of energy spectra were investigated. A similar definition of the effective rotation term was found to be more appropriate than either the Coriolis term or rotation-induced pressure term for representing the effect of the streamwise system rotation on the flow dynamics. Different from our previous study, which focuses on the normal components of energy spectra, the present study aims to investigate the reversal behavior of Reynolds shear stress $\langle u'_2 u'_3 \rangle$ by analyzing its budget balance in the physical space.

Figure 4 compares the profiles of budget terms in the transport equation of Reynolds shear stress $\langle u'_2 u'_3 \rangle^+$ at $Ro_\tau = 7.5$ (the lowest rotation number for the rotating channel flow under investigation), $Ro_\tau = 30$ (the critical rotation number at which the magnitude of $\langle u'_2 u'_3 \rangle^+$ reverses, see Fig. 3), and $Ro_\tau = 150$ (the highest rotation number under investigation). To ensure that the flow is developed to a statistically stationary state, it is useful to examine the residual of the summation of all budget terms in Eq. (4), which is found to be smaller than 1% of the dominant source terms in all cases under investigation. Furthermore, the time averaging in the present study is conducted over a time duration of $T = 50h/u_\tau$. We have also calculated the budget terms by reducing the averaging time duration to $T = 25h/u_\tau$, which does not cause any increase in the residual magnitude. This indicates that the averaging time is sufficiently long, and the error is mainly attributed to the spatial discretization, but not the assumption that the flow is statistically stationary. From Fig. 4(a), it is clear that the convection-induced pressure term Π_{23}^{c+} and effective rotation term $C_{23}^{\text{eff}+}$ are two dominant sources of $\langle u'_2 u'_3 \rangle^+$ at $Ro_\tau = 7.5$. At all three rotation numbers, the convection-induced pressure term Π_{23}^{c+} acts as an important source, and its effect becomes increasingly dominant as the rotation number increases. Furthermore, by comparing Figs. 4(a)–4(c), it is seen that the effect of $C_{23}^{\text{eff}+}$ (as a gain for $\langle u'_2 u'_3 \rangle^+$) is the most apparent at $Ro_\tau = 30$.

To further investigate the effective rotation term $C_{23}^{\text{eff}+}$, we compare its profiles at various rotation numbers, together with the Coriolis term C_{23}^+ [Eq. (11)] and rotation-induced pressure term Π_{23}^r [Eq. (12)] in Fig. 5. It is seen from Fig. 5(b) that the Coriolis term C_{23}^+

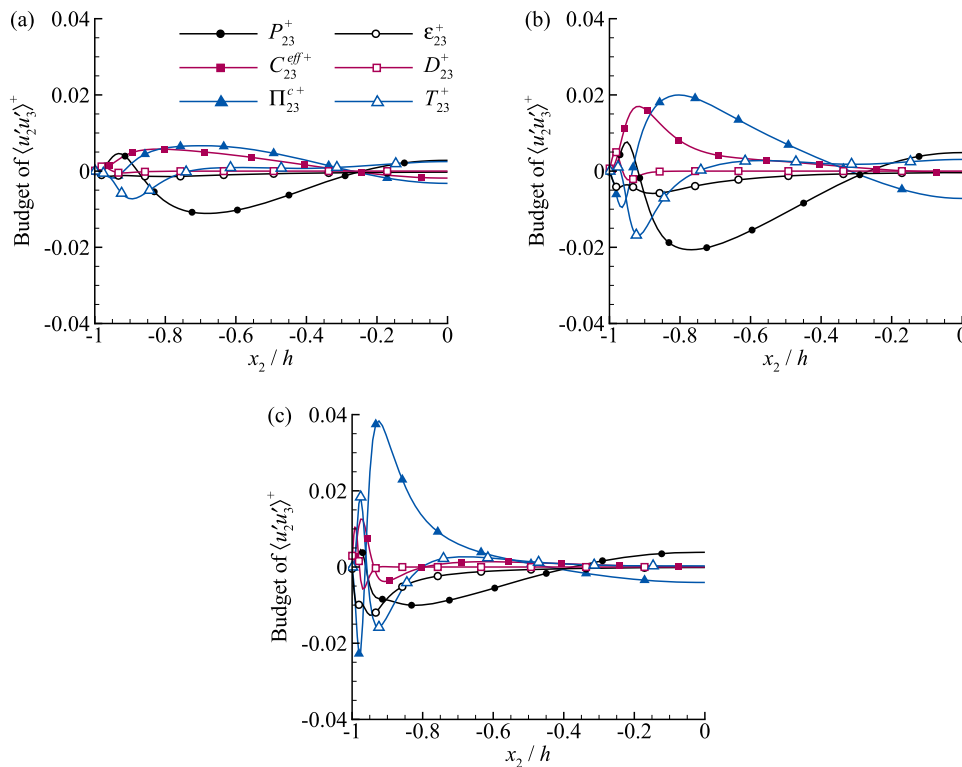


FIG. 4. Profiles of budget terms in the transport equation of Reynolds shear stress $\langle u'_2 u'_3 \rangle^+$ in the streamwise-rotating turbulent channel flow at (a) $Ro_\tau = 7.5$, (b) $Ro_\tau = 30$, and (c) $Ro_\tau = 150$.

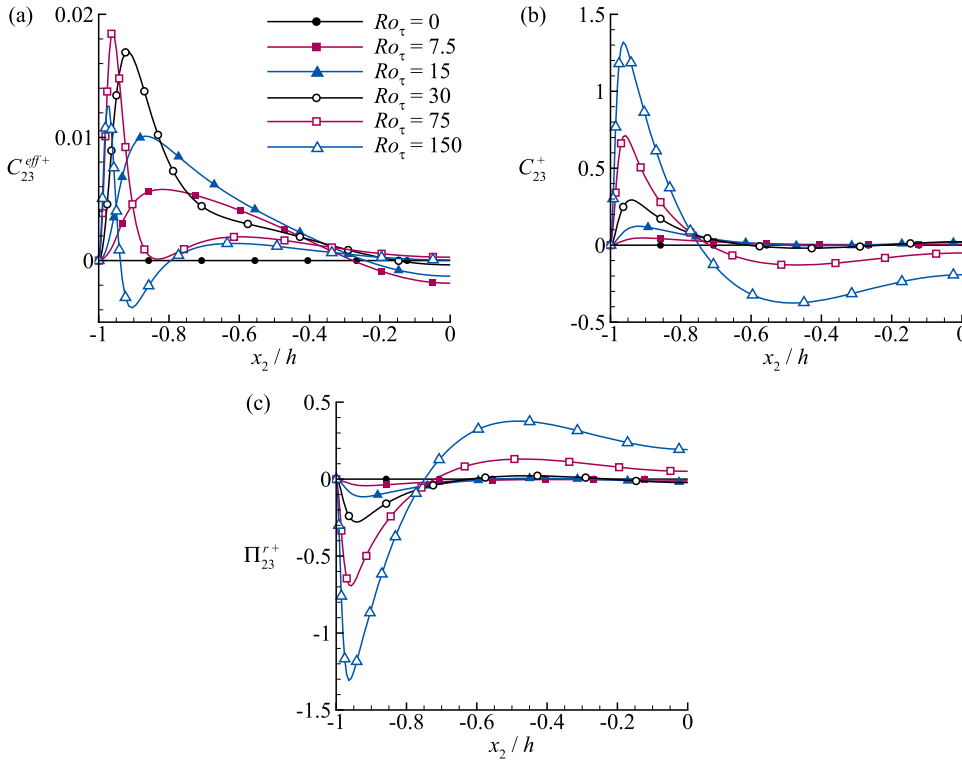


FIG. 5. Profiles of (a) effective rotation term C_{23}^{eff+} , (b) Coriolis term C_{ij}^+ , and (c) rotation-induced pressure term Π_{ij}^{r+} at various rotation numbers.

is positively valued in the near-wall region, while in the core region of the channel, the value of C_{23}^+ is negative at high rotation numbers ($Ro_\tau = 75$ and 150). The sign of C_{23}^+ can be understood from its definition, expressed as

$$C_{23}^+ = Ro_\tau (\langle u'_3 u'_3 \rangle^+ - \langle u'_2 u'_2 \rangle^+). \quad (15)$$

In the near wall region, due to the restriction of the wall, the magnitude of $\langle u'_2 u'_2 \rangle^+$ is smaller than that of $\langle u'_3 u'_3 \rangle^+$, leading to the positive value of C_{23}^+ . At high rotation numbers, the occurrence of intensive large-scale Taylor-Görtler-like vortices enhances the wall-normal velocity fluctuation u'_2 in the core region of the channel,¹⁷ and consequently, the sign of C_{23}^+ becomes negative there. The rotation-induced pressure term Π_{23}^{r+} depicted in Fig. 5(c) almost form a mirror image of C_{23}^+ at all rotation numbers under investigation. This indicates that these two rotation-induced terms C_{23}^+ and Π_{23}^{r+} mostly cancel the effect of each other, leaving a significantly smaller net effect of the imposed system rotation on the budget balance of $\langle u'_2 u'_3 \rangle^+$. As a result, although the magnitudes of both C_{ij}^+ and Π_{ij}^{r+} increase approximately in a linear approach with respect to the rotation number (a phenomenon that can be understood from the definitions of C_{ij}^+ and Π_{ij}^{r+}), the net effect of the system rotation on $\langle u'_2 u'_3 \rangle^+$ as represented by the effective rotation term C_{23}^{eff+} is non-monotonic. As shown in Fig. 5(a), the peak value of C_{23}^{eff+} reaches its maximum at $Ro_\tau = 75$. This rotation number is higher than the critical reversal rotation number of $\langle u'_2 u'_3 \rangle^+$ ($Ro_\tau = 30$ as shown in Fig. 3), indicating that the effect of C_{23}^{eff+} is important, but meanwhile not primary, in the non-monotonically behavior of $\langle u'_2 u'_3 \rangle^+$.

Another term that plays a crucial role in the magnitude-reverse phenomenon of $\langle u'_2 u'_3 \rangle^+$ is the production term P_{23}^+ . As shown in Fig. 4, the profiles of the production term P_{23}^+ are complex. From Eq. (5), we obtain

$$P_{23}^+ = -\langle u'_2 u'_2 \rangle^+ \frac{d\langle u_3 \rangle^+}{dx_2^+}, \quad (16)$$

from which it can be inferred that the profile of P_{23}^+ must cross zero six times in the wall-normal direction of the channel (for $-1 \leq x_2/h \leq 1$) or, equivalently, three times in the lower half of the channel (for $-1 \leq x_2/h \leq 0$), as shown in Fig. 4. Owing to the wall restriction, $P_{23}^+ = 0$ holds at the two walls (i.e., at $x_2/h = \pm 1$). Furthermore, as shown in Fig. 2, there are four layers of opposite mean spanwise motion $\langle u_3 \rangle^+$. In each layer, there exists a wall-normal position x_2 where the magnitude of the spanwise velocity $\langle u_3 \rangle^+$ reaches its local maximum, where $d\langle u_3 \rangle^+/dx_2^+ = 0$ holds. Therefore, the other four zero points of P_{23}^+ collocate with the four peaks of $\langle u_3 \rangle^+$. In summary, given the four distinct layers of the opposite mean spanwise motion, the sign of P_{23}^+ must change four times in the entire channel.

It is seen from Fig. 4 that the value of P_{23}^+ is mostly negative across the wall-normal direction (e.g., at $Ro_\tau = 30$, $P_{23}^+ < 0$ holds in the region for $-0.92 \leq x_2/h \leq -0.27$). This indicates that P_{23}^+ serves as a sink in the transport equation of $\langle u'_2 u'_3 \rangle^+$, which tends to suppress the magnitude of this Reynolds shear stress component. By comparing Figs. 4(a)–4(c), it is clear that the magnitude of the negatively valued peak of P_{23}^+ is the largest at $Ro_\tau = 30$ among the three rotation numbers. To demonstrate this trend more clearly, the profiles of P_{23}^+ at six rotation numbers are compared in Fig. 6. Similar to $\langle u'_2 u'_3 \rangle^+$, the magnitude of the negatively valued peak of P_{23}^+ also reverses at

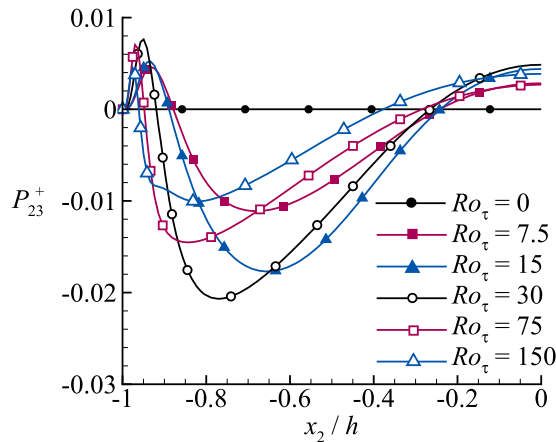


FIG. 6. Profiles of the production term P_{23}^+ at various rotation numbers.

$Ro_\tau = 30$. From Eq. (5), we obtain

$$P_{23}^+ = -\langle u'_2 u'_3 \rangle^+ \frac{d\langle u_3 \rangle^+}{dx_2^+}. \quad (17)$$

Substituting Eq. (3) into (17) results in

$$P_{23}^+ = -\langle u'_2 u'_3 \rangle^+ \left(\langle u'_2 u'_3 \rangle^+ + \tau_{23}^{\text{wall}+} \right). \quad (18)$$

Given the fact that $\langle u'_2 u'_3 \rangle^+$ is positive semi-definite, Eq. (18) indicates that $\langle u'_2 u'_3 \rangle^+$ always imposes a negative net feedback to itself through its production term P_{23}^+ . To be specific, as the rotation number increases from 0 to 30, accompanied with the magnitude increase in $\langle u'_2 u'_3 \rangle^+$, the suppression effect of the production term P_{23}^+ becomes stronger. This “self-constraint” mechanism prevents the magnitude of $\langle u'_2 u'_3 \rangle^+$ from monotonically increasing as the rotation number continues to increase, and as a result, the magnitude of $\langle u'_2 u'_3 \rangle^+$ shows a non-monotonic behavior in Fig. 3.

The magnitude reverse phenomenon of the near-wall peak of $\langle u_3 \rangle^+$ with respect to an increasing rotation number is coupled with that of $\langle u'_2 u'_3 \rangle^+$. To demonstrate it, we integrate Eq. (3) from $-h^+$ to h^+ . Further considering the no-slip condition at the two walls and the symmetry in the profile of $\langle u'_2 u'_3 \rangle^+$ about the channel center ($x_2/h = 0$), we obtain

$$\tau_{23}^{\text{wall}+} = -\frac{1}{h^+} \int_{-h^+}^0 \langle u'_2 u'_3 \rangle^+ dx_2^+. \quad (19)$$

From Eq. (19), it is understood that the value of $\tau_{23}^{\text{wall}+}$ is proportional to the integration of $\langle u'_2 u'_3 \rangle^+$ over the lower half of the channel. Figure 3 shows that the magnitude of $\langle u'_2 u'_3 \rangle^+$ reverses at $Ro_\tau = 30$, and consequently, $\tau_{23}^{\text{wall}+}$ also reverses at $Ro_\tau = 30$. In the near-wall region, the mean spanwise velocity can be expanded into Taylor series as

$$\langle u_3 \rangle^+ = \frac{d\langle u_3 \rangle^+}{dx_2^+} \bigg|_{x_2^+ = -h^+} y^+ + \mathcal{O}(y^{+2}) = \tau_{23}^{\text{wall}+} y^+ + \mathcal{O}(y^{+2}), \quad (20)$$

indicating that the behaviors of the near-wall peak of $\langle u_3 \rangle^+$ and $\tau_{23}^{\text{wall}+}$ must synchronize in response to an increasing rotation number. As a result, the near-wall peak of $\langle u_3 \rangle^+$ also reverses at the same rotation number (see Fig. 2).

V. CONCLUSIONS

In this paper, we investigate the mechanism underlying the non-monotonic behavior of the cross-stream secondary flow $\langle u_3 \rangle$ with respect to an increasing rotation number in the streamwise-rotating turbulent channel flow. Using the DNS data, it is demonstrated that the magnitudes of both $\langle u_3 \rangle$ and $\langle u'_2 u'_3 \rangle$ reverse at $Ro_\tau = 30$. Through the analysis of the transport equation of $\langle u'_2 u'_3 \rangle$, it is found that $\langle u'_2 u'_3 \rangle$ imposes a negative feedback to itself through the production term P_{23} . This self-constraint mechanism prevents the magnitude of $\langle u'_2 u'_3 \rangle$ from increasing monotonically in response to an increasing rotation number. The effective rotation term plays a secondary role in the magnitude reverse of $\langle u'_2 u'_3 \rangle$. The two components of the effective rotation term, namely, the Coriolis term and rotation-induced pressure term, both increase approximately in a linear approach with respect to the rotation number. However, their effects mostly cancel each other, leaving a significantly smaller net effect on the budget balance of $\langle u'_2 u'_3 \rangle$ as represented by the effective rotation term. The peak value of the effective rotation term reverses at $Ro_\tau = 75$, larger than the critical reversal rotation number of $\langle u'_2 u'_3 \rangle$. Due to the linear relationship between the spanwise wall shear stress τ_{23}^{wall} and the integration of $\langle u'_2 u'_3 \rangle$, the value of τ_{23}^{wall} also reverses at $Ro_\tau = 30$. Furthermore, through a Taylor-series analysis, it is shown that the near-wall behavior of $\langle u_3 \rangle$ depends linearly on that of τ_{23}^{wall} . As such, the magnitude-reverse phenomenon of $\langle u_3 \rangle$ is explained.

ACKNOWLEDGMENTS

Z.Y. would like to thank the support of the NSFC Basic Science Center Program for “Multiscale Problems in Nonlinear Mechanics” (Grant No. 11988102) and the Lixing research funding of Institute of Mechanics, Chinese Academy of Sciences. The DNS database was established under the support of the Natural Sciences and Engineering Research Council (NSERC) of Canada to B.-C.W.

DATA AVAILABILITY

Raw data were generated at the Western Canada Research Grid (WestGrid) large scale facility. The data that support the findings of this study are available from the corresponding author upon reasonable request.

REFERENCES

- H. Wu and N. Kasagi, “Effects of arbitrary directional system rotation on turbulent channel flow,” *Phys. Fluids* **16**, 979–990 (2004).
- M. Oberlack, W. Cabot, B. A. P. Reif, and T. Weller, “Group analysis, direct numerical simulation and modelling of a turbulent channel flow with streamwise rotation,” *J. Fluid Mech.* **562**, 383–403 (2006).
- T. Weller and M. Oberlack, “DNS of a turbulent channel flow with streamwise rotation—Investigation on the cross flow phenomena,” in *Direct and Large-Eddy Simulation VI*, edited by E. Lamballais, R. Friedrich, B. J. Geurts, and O. Métais (Springer, 2006), pp. 241–248.
- T. Weller and M. Oberlack, “DNS of a turbulent channel flow with streamwise rotation—Study of the reverse effect of the cross flow,” *Proc. Appl. Math. Mech.* **6**, 553–554 (2006).
- I. Recktenwald, T. Weller, W. Schröder, and M. Oberlack, “Comparison of direct numerical simulations and particle-image velocimetry data of turbulent channel flow rotating about the streamwise axis,” *Phys. Fluids* **19**, 085114 (2007).

- ⁶N. Alkishriwi, M. Meinke, and W. Schröder, “Large-eddy simulation of streamwise-rotating turbulent channel flow,” *Comput. Fluids* **37**, 786–792 (2008).
- ⁷I. Recktenwald, N. Alkishriwi, and W. Schröder, “PIV-LES analysis of channel flow rotating about the streamwise axis,” *Eur. J. Mech.: B/Fluids* **28**, 677–688 (2009).
- ⁸B.-C. Wang and Y. Zhang, “Large-eddy simulation of turbulent flows in a heated streamwise rotating channel,” *Int. J. Heat Fluid Flow* **44**, 71–86 (2013).
- ⁹Y.-J. Dai, W.-X. Huang, and C.-X. Xu, “Coherent structures in streamwise rotating channel flow,” *Phys. Fluids* **31**, 021204 (2019).
- ¹⁰S. Masuda, S. Fukuda, and M. Nagata, “Instabilities of plane Poiseuille flow with a streamwise system rotation,” *J. Fluid Mech.* **603**, 189–206 (2008).
- ¹¹Y.-T. Yang, W.-D. Su, and J.-Z. Wu, “Helical-wave decomposition and applications to channel turbulence with streamwise rotation,” *J. Fluid Mech.* **662**, 91–122 (2010).
- ¹²N. N. Mansour, J. Kim, and P. Moin, “Reynolds-stress and dissipation-rate budgets in a turbulent channel flow,” *J. Fluid Mech.* **194**, 15–44 (1988).
- ¹³J. Komminaho and M. Skote, “Reynolds stress budgets in Couette and boundary layer flows,” *Flow, Turbul. Combust.* **68**, 167–192 (2002).
- ¹⁴S. Hoyas and J. Jiménez, “Reynolds number effects on the Reynolds-stress budgets in turbulent channels,” *Phys. Fluids* **20**, 101511 (2008).
- ¹⁵V. Avsarkisov, S. Hoyas, M. Oberlack, and J. P. García-Galache, “Turbulent plane Couette flow at moderately high Reynolds number,” *J. Fluid Mech.* **751**, R1 (2014).
- ¹⁶T. Kawata and P. H. Alfredsson, “Scale interactions in turbulent rotating planar Couette flow: Insight through the Reynolds stress transport,” *J. Fluid Mech.* **879**, 255–295 (2019).
- ¹⁷Z. Yang, B.-Q. Deng, B.-C. Wang, and L. Shen, “Sustaining mechanism of Taylor–Görtler-like vortices in a streamwise-rotating channel flow,” *Phys. Rev. Fluids* **5**, 044601 (2020).
- ¹⁸Z. Yang and B.-C. Wang, “Capturing Taylor–Görtler vortices in a streamwise-rotating channel at very high rotation numbers,” *J. Fluid Mech.* **838**, 658–689 (2018).
- ¹⁹Z. Yang, B.-Q. Deng, B.-C. Wang, and L. Shen, “Letter: The effects of streamwise system rotation on pressure fluctuations in a turbulent channel flow,” *Phys. Fluids* **30**, 091701 (2018).
- ²⁰K. Nakabayashi and O. Kitoh, “Turbulence characteristics of two-dimensional channel flow with system rotation,” *J. Fluid Mech.* **528**, 355–377 (2005).
- ²¹N.-S. Liu and X.-Y. Lu, “A numerical investigation of turbulent flows in a spanwise rotating channel,” *Comput. Fluids* **36**, 282–298 (2007).
- ²²O. Grundestam, S. Wallin, and A. V. Johansson, “Direct numerical simulations of rotating turbulent channel flow,” *J. Fluid Mech.* **598**, 177–199 (2008).
- ²³T. Kawata and P. H. Alfredsson, “Experiments in rotating plane Couette flow—Momentum transport by coherent roll-cell structure and zero-absolute-vorticity state,” *J. Fluid Mech.* **791**, 191–213 (2016).
- ²⁴T. Kawata and P. H. Alfredsson, “Turbulent rotating plane Couette flow: Reynolds and rotation number dependency of flow structure and momentum transport,” *Phys. Rev. Fluids* **1**, 034402 (2016).